

A thermodynamically complete multi-phase equation of state for dense and porous metals at wide ranges of temperature and pressure

Yanhong Zhao(赵艳红)†, Li-Fang Wang(王丽芳)†, Qili Zhang(张其黎), Le Zhang(张乐), Hongzhou Song(宋红州), Xingyu Gao(高兴誉), Bo Sun(孙博), Haifeng Liu(刘海风), and Haifeng Song(宋海峰)‡

Citation: Chin. Phys. B, 2025, 34 (**3**): 036401. DOI: 10.1088/1674-1056/ada54b
Journal homepage: http://cpb.iphy.ac.cn; http://iopscience.iop.org/cpb

What follows is a list of articles you may be interested in

A high-pressure study of Cr_3C_2 by XRD and DFT

Lun Xiong(熊伦), Qiang Li(李强), Cheng-Fu Yang(杨成福), Qing-Shuang Xie(谢清爽), Jun-Ran Zhang(张俊然)
Chin. Phys. B, 2020, 29 (**8**): 086401. DOI: 10.1088/1674-1056/ab8c3d

Equation of state of $LiCoO_2$ under 30 GPa pressure

Yong-Qing Hu(户永清), Lun Xiong(熊伦), Xing-Quan Liu(刘兴泉), Hong-Yuan Zhao(赵红远), Guang-Tao Liu(刘广涛), Li-Gang Bai(白利刚), Wei-Ran Cui(崔巍然), Yu Gong(宫宇), Xiao-Dong Li(李晓东)
Chin. Phys. B, 2019, 28 (**1**): 016402. DOI: 10.1088/1674-1056/28/1/016402

Equation of state for aluminum in warm dense matter regime

Kun Wang(王坤), Dong Zhang(张董), Zong-Qian Shi(史宗谦), Yuan-Jie Shi(石元杰), Tian-Hao Wang(王天浩), Yue Zhang(张阅)
Chin. Phys. B, 2019, 28 (**1**): 016401. DOI: 10.1088/1674-1056/28/1/016401

Anomalous behavior and phase transformation of α-GaOOH nanocrystals under static compression

Zhao Zhang(张钊), Hang Cui(崔航), Da-Peng Yang(杨大鹏), Jian Zhang(张剑), Shun-Xi Tang(汤顺熙), Si Wu(吴思), Qi-Liang Cui(崔啟良)
Chin. Phys. B, 2017, 26 (**10**): 106402. DOI: 10.1088/1674-1056/26/10/106402

Structure phase transformation and equation of state of cerium metal under pressures up to 51 GPa

Ce Ma(马策), Zuo-Yong Dou(窦作勇), Hong-Yang Zhu(祝洪洋), Guang-Yan Fu(付广艳), Xiao Tan(谈笑), Bin Bai(白彬), Peng-Cheng Zhang(张鹏程), Qi-Liang Cui(崔啟良)
Chin. Phys. B, 2016, 25 (**4**): 046401. DOI: 10.1088/1674-1056/25/4/046401

A thermodynamically complete multi-phase equation of state for dense and porous metals at wide ranges of temperature and pressure

Yanhong Zhao(赵艳红)[†], Li-Fang Wang(王丽芳)[†], Qili Zhang(张其黎), Le Zhang(张乐), Hongzhou Song(宋红州), Xingyu Gao(高兴誉), Bo Sun(孙博), Haifeng Liu(刘海风), and Haifeng Song(宋海峰)[‡]

National Key Laboratory of Computational Physics, Institute of Applied Physics and Computational Mathematics, Beijing 100094, *China*

(Received 21 October 2024; revised manuscript received 2 January 2025; accepted manuscript online 3 January 2025)

A thermodynamically complete multi-phase equation of state (EOS) applicable to both dense and porous metals at wide ranges of temperature and pressure is constructed. A standard three-term decomposition of the Helmholtz free energy as a function of specific volume and temperature is presented, where the cold component models both compression and expansion states, the thermal ion component introduces the Debye approximation and melting entropy, and the thermal electron component employs the Thomas–Fermi–Kirzhnits (TFK) model. The porosity of materials is considered by introducing the dynamic porosity coefficient α and the constitutive P–α relation, connecting the thermodynamic properties between dense and porous systems, allowing for an accurate description of the volume decrease caused by void collapse while maintaining the quasi-static thermodynamic properties of porous systems identical to the dense ones. These models enable the EOS applicable and robust at wide ranges of temperature, pressure and porosity. A systematic evaluation of the new EOS is conducted with aluminum (Al) as an example. 300 K isotherm, shock Hugoniot, as well as melting curves of both dense and porous Al are calculated, which shows great agreements with experimental data and validates the effectiveness of the models and the accuracy of parameterizations. Notably, it is for the first time Hugoniot P–σ curves up to 10^6 GPa and shock melting behaviors of porous Al are derived from analytical EOS models, which predict much lower compression limit and shock melting temperatures than those of dense Al.

Keywords: equation of state, multi-phase model, porous metal

PACS: 64.10.+h, 64.30.Ef, 64.90.+b

DOI: 10.1088/1674-1056/ada54b **CSTR:** 32038.14.CPB.ada54b

1. Introduction

The equations of state (EOS), which define the thermodynamic properties of matter over a wide range of temperatures and pressures, play a key role in many fields, including aerospace, astrophysics, geophysics, and shock physics.[1] They are particularly important for predicting the dynamic behaviors of matters under extreme conditions by solving the conservation equations for mass, momentum, and energy. Specifically, physical models of EOS greatly influence the plausibility and applicability of the simulations, as they describe how the different matters respond to external or internal loading. For decades, numerous well-known EOS models and functionals have been established, such as the Mie–Gruneisen EOS,[2,3] the quotidian EOS,[4] the Birch potential based EOS,[5] the LANL Sesame EOS,[6] the wide-regime EOS,[7] and so on. Among them, the semi-empirical EOS models, of which functional forms are motivated by physical insights and the parameters are optimized to experimental as well as theoretical data,[7] have been proven accurate in wide ranges of pressure and temperature.[4,6,7] As a result, these models serve as the foundation for the construction of various multi-phase EOSs. Based on a comprehensive understanding of the phase diagrams, high-precision multi-phase EOSs have been developed for various materials, including platinum,[8,9] iron,[10] aluminum (Al),[11] beryllium,[12] carbon,[13] titanium,[14] and Ti alloys.[15] However, these EOS models and functionals are only applicable for ideal and dense matters, while the effects of pre-existing heterogeneities in materials are neglected.

In recent years, the growing need to understand the relationship between material structure, properties, and performance under extreme conditions has highlighted the importance and urgency of developing wide-range EOS models that can accurately capture multi-phase characteristics and account for the heterogeneous nature of practical materials. Specifically, pre-existing voids, one of the most important microstructures in materials, have been found to significantly influence material behaviors under dynamic loading.[16] Thus, it is important to incorporate porosity characterization into EOS models to make them applicable for porous materials. Unfortunately, the majority of existing porous EOS models are limited to single-phase models and can only be applied up to a few hundred GPa.[17–25] As porous materials are more likely to undergo phase transitions[26,27] and are used in a wide range of temperature and pressure conditions,[28] it is necessary to develop multi-phase equations of states that can accommodate

[†]These authors contributed equally to this work.

[‡]Corresponding author. E-mail: song_haifeng@iapcm.ac.cn

© 2025 Chinese Physical Society and IOP Publishing Ltd. All rights, including for text and data mining, AI training, and similar technologies, are reserved.

such materials.

Therefore, in this work, we establish a multi-phase equation of state applicable for both dense and porous metals at wide ranges of temperature and pressure. In Section 2, a detailed description of models is provided. In Section 3, systematic evaluations of the new EOS are conducted with Al as prototype. Finally, conclusions are presented in Section 4.

2. Models

2.1. EOS models for dense system

In order to construct a thermodynamically complete equation of state, a standard three-term decomposition of the Helmholtz free energy as a function of specific volume and temperature is employed. It is expressed as follows:

$$F(V,T) = F_{\rm c}(V) + F_{\rm n}(V,T) + F_{\rm e}(V,T), \tag{1}$$

where $F_{\rm c}(V)$, $F_{\rm n}(T,V)$, and $F_{\rm e}(T,V)$ represent the cold, thermal ion and thermal electron components, respectively. This model enables the derivation of all additional thermodynamic quantities of the material systems once the EOS is determined.

For $F_{\rm c}(V)$, two functional models are employed to calculate the total energy of the system at the temperature of 0 K. In the compression situation, where the cold compression ratio $\sigma_{\rm c} \geq 1$, a polynomial function is applied, and the cold free energy is expressed as[29]

$$F_{\rm c1} = 3V_{0\rm C}\sum_{i=1}^{5}\frac{a_i}{i}\left(\sigma_{\rm c}^{i/3}-1\right), \quad (\sigma_{\rm c}\geq 1), \tag{2}$$

where $V_{0\rm C}$ represents the equilibrium volume of the system at 0 K, and a_i are the coefficients which need to be fitted. In the expansion situation, where $\sigma_{\rm c} < 1$, the Lennard–Jones potential is utilized to characterize the atomic interaction in the system. Thus, the cold free energy can be written as[29]

$$F_{\rm c2} = V_{0\rm C}\left\{A\left[\frac{1}{k}\sigma_{\rm c}^{k}-\frac{1}{l}\sigma_{\rm c}^{l}\right]+B\left[\frac{1}{n}\sigma_{\rm c}^{n}-\frac{1}{l}\sigma_{\rm c}^{l}\right]\right\}+E_{\rm sub}, \quad (\sigma_{\rm c}<1), \tag{3}$$

where A, B, k, l, and n are the model parameters, and $E_{\rm sub}$ is the cohesive energy of the system at ambient conditions. Constraint conditions:

$$F(\sigma_{\rm c}=0) = E_{\rm sub}, \tag{4}$$

$$P(\sigma_{\rm c}=1) = 0, \tag{5}$$

$$F_{\rm c1} = F_{\rm c2}, (\sigma_{\rm c}=1), \tag{6}$$

$$F'_{\rm c1} = F'_{\rm c2}, (\sigma_{\rm c}=1) \tag{7}$$

are employed to make sure the $F_{\rm c}(V)$ model physically plausible and numerically continuous and smooth. The parameters of the cold curve component, including a_i, A, B, k, l, n and $E_{\rm sub}$, are determined through fitting the results from DFT calculations and the solutions of the Thomas–Fermi–Kirzhnits (TFK) model.

For $F_{\rm n}(T,V)$, solid and liquid phase models are respectively constructed. For the solid phase, a Debye approximation is employed:[30]

$$F_{\rm n}^{(\rm S)}(V,T) = NKT\left[\frac{9}{8}\frac{\theta}{T}+3\ln\left(1-{\rm e}^{-\theta/T}\right)-D\left(\frac{\theta}{T}\right)\right], \tag{8}$$

$$D(x) = \frac{3}{x^3}\int_0^x \frac{y^3}{{\rm e}^y-1}{\rm d}y, \tag{9}$$

where θ is the Debye temperature as a function of the specific volume. Thus, the pressure and energy of the system could be derived as

$$E_{\rm n}^{(\rm S)}(V,T) = NKT\left[\frac{9}{8}\frac{\theta}{T}+3D\left(\frac{\theta}{T}\right)\right], \tag{10}$$

$$P_{\rm n}^{(\rm S)}(V,T) = \frac{\Gamma E_{\rm n}^{(\rm S)}(V,T)}{V}, \tag{11}$$

where $\Gamma = \chi + \frac{\beta}{\rho}$, χ and β are the parameters to be determined through Hugoniot experiment data. The approximation model of Γ employed in this work is referenced in Ref. [54]. As explained in this reference, this form of the Gruneisen parameter enables us to satisfy a well-known infinite-compression limit derived for the one-component plasma if α is chosen to be $1/2$. This model has also been successfully utilized in other works, including the construction of a multi-phase equation of state for beryllium[55] and carbon.[56]

For the liquid phase, the melting entropy is considered, thus the free energy contributed by the thermal ions could be expressed as

$$F_{\rm n}^{(\rm L)}(V,T) = F_{\rm n}^{(\rm S)}(V,T) + NKT(F_0+F_1), \tag{12}$$

$$F_0 = \frac{3}{2}\ln\psi+\delta_1+\frac{\delta_2}{\left[\psi^y\left(\delta_3+\psi^{1-y}\right)\right]}+\frac{\delta_4\left[1-\frac{3}{8\psi^{\frac{1}{2}}}\right]}{\psi^{\frac{3}{2}}}, \tag{13}$$

$$F_1 = \frac{0.66}{\psi}-0.6. \tag{14}$$

In this way, the pressure and energy of the liquid system could be derived as

$$E_{\rm n}^{(\rm L)}(V,T) = E_{\rm n}^{(\rm S)}(V,T) + NKT(E_0+E_1), \tag{15}$$

$$P_{\rm n}^{(\rm L)}(V,T) = \frac{\left[\Gamma E_{\rm n}^{(\rm S)}(V,T)+NKT\left(2\Gamma-\frac{2}{3}\right)(E_0+E_1)\right]}{V}, \tag{16}$$

with

$$E_0 = -\frac{3}{2}+\frac{3}{2}\delta_4\left[1-1/(2\psi^{\frac{1}{2}})\right]/\psi^{\frac{3}{2}} + \delta_2\left(\delta_3 y+\psi^{1-y}\right)/\left[\psi^y\left(\delta_3+\psi^{1-y}\right)^2\right], \tag{17}$$

$$E_1 = \frac{0.66}{\psi}, \tag{18}$$

where $\psi, y, \delta_1, \delta_2, \delta_3, \delta_4$ are referenced in Ref. [30]. This fluidic model smoothly transitions from the liquid phase to the

ideal gas phase, with the specific heat monotonically decreasing from approximately $3R$ to $3R/2$ at high temperatures, and successfully describes the thermodynamic properties of ions over wide pressure and temperature ranges.

Finally, for the electronic thermal component $F_e(T,V)$, a quadratic form expansion of the TFK model is employed at lower temperatures as follows:[31]

$$F_e^s(V,T) = -\frac{1}{2}\beta_{0K}\left(\frac{V}{V_0}\right)^{\frac{1}{2}}T^2, \tag{19}$$

where β_{0K} is the specific heat coefficient of electrons determined by the experimental data of specific heat capacity of crystals; while at higher temperatures, explicit formulas of TFK model[31] are employed, which could accurately describe the behavior of thermal electrons by inducing the exchange–correlation and quantum effects.

2.2. Constitutive models for porous system

Based on the EOS models of dense materials as presented above, constitutive models of porous materials are introduced, in order to enable the EOS to be applied for both dense and porous systems. Ignoring the surface effects of porous morphology, a dynamic porosity coefficient, α, is introduced to establish a relationship of thermodynamic properties between dense and porous materials. The dynamic porosity coefficient could be expressed as follows:

$$\alpha = \frac{V}{V_s}. \tag{20}$$

Thus, the pressure and energy of the porous materials could be derived as

$$P(V,T) = P_s(V_s,T) = P_s\left(\frac{V}{\alpha},T\right), \tag{21}$$

$$E(V,T) = E_s(V_s,T) = E_s\left(\frac{V}{\alpha},T\right), \tag{22}$$

where P_s, E_s, and V_s are the pressure, energy and molar volume of the dense system, respectively. Normally, α is a function of pressure and temperature variables. In this study, we assume that the dynamic porosity α mainly depends on pressure,

$$\alpha = \alpha(P,T) \approx \alpha(P), \tag{23}$$

then it could be derived by the P–α model, which was developed by Herrmann and Cornell *et al.*[32,33] as follows:

$$\alpha = \begin{cases} m, & 0 < P < P_e, \\ \frac{1}{1-\exp\left(-\frac{3P}{2Y}\right)}, & P_e < P < \infty, \end{cases} \tag{24}$$

where m is the initial porosity of the system, P_e is the elastic Hugoniot limit:

$$m = \frac{\rho_{s0}}{\rho_0}, \tag{25}$$

$$P_e = \frac{2}{3}Y\ln\left(\frac{m}{m-1}\right), \tag{26}$$

where ρ_{s0} and Y are the initial density and the Hugoniot elastic limit of the dense system, respectively. In this way, by solving the dynamical porosity coefficient α, the EOS of the porous system could be derived.

2.3. Phase boundary calculation

The phase boundaries are derived from the EOS model based on the assumption of pressure equilibrium, temperature equilibrium and Gibbs free energy equilibrium:

$$T^{\text{phase1}} = T^{\text{phase2}} = T, \tag{27}$$

$$P^{\text{phase1}}(V_1,T) = P^{\text{phase2}}(V_2,T) = P, \tag{28}$$

$$G^{\text{phase1}}(P,T) = G^{\text{phase2}}(P,T). \tag{29}$$

Then, by using a mixture method, the energy and specific volume of the system along the phase boundaries could be expressed as

$$E(V,T) = (1-\lambda)\cdot E^{\text{phase1}}(V_1,T) + \lambda\cdot E^{\text{phase2}}(V_2,T), \tag{30}$$

$$V = (1-\lambda)\cdot V_1 + \lambda\cdot V_2, \tag{31}$$

where λ is the molar fraction of the phase and the subscripts 1 and 2 refer to phases 1 and 2, respectively. Other thermodynamic properties along the phase boundary could be derived accordingly.

3. Results and discussion

In this section, a systematic evaluation of the new EOS is conducted with Al as prototype. Wide range isotherm curves, shock Hugoniots, and melt curves for both dense and porous Al are derived based on the new EOS. To validate the models and parameters of the new EOS, experimental results are also presented for comparison.

3.1. Isotherm curves

Currently, although the isothermal compression curve at 0 K cannot be directly measured in experiments, the isothermal compression curve at 300 K can be precisely measured. These experiments typically use diamond anvil cells to apply pressure to the samples and utilize synchrotron radiation facilities to measure the lattice parameters; thus, the relationship between pressure and density of the samples can be obtained. The pressure measured along the 300 K isothermal compression curve closely matches that measured along the 0 K isothermal compression curve, making it important reference data for verifying the validity of cold compression component.

The 300 K isotherm curves of dense and porous Al are derived, as shown in Fig. 1. For the dense Al, the comparison of calculations with available experimental data[34,35]

shows good consistency, confirming the accuracy of the models and parameterizations of the EOS cold components. For the porous Al, the isothermal compression curves demonstrate a three-stage process, starting with the elastic deformation, followed by the plastic deformation due to void collapse, and finally exhibiting the volume compression under isotherm conditions. It is worth noting that once densified, all the porous Al exhibit the same P–ρ isotherm curve as dense Al, indicating that the dense and porous materials undergo the same quasi-static process under higher pressures.

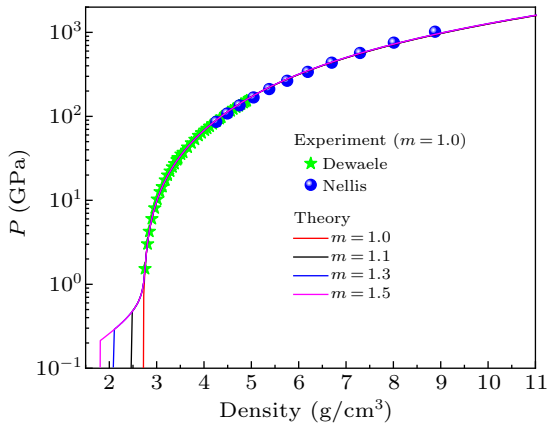


Fig. 1. The 300 K isotherm curves of dense and porous Al with different initial porosity m. The lines are results derived based on the new EOS and dots are published experimental results.[34,35]

3.2. Shock Hugoniots

Experimental shock Hugoniot data is an important reference for validating the total pressure and energy of the equation of state. In these experiments, shock wave velocity, particle velocity, and shock pressure could be measured carefully, thus the Hugoniot curve of the materials could be obtained.

Theoretically, thermodynamic properties behind the shock front are calculated with the Rankine–Hugoniot equation

$$E - E_0 = \frac{1}{2}(P + P_0)(V_0 - V), \tag{32}$$

where V_0, P_0, E_0 are the initial volume, pressure, energy of the material before the shock loading, respectively, while V, P, E are the final volume, pressure, energy of the material after the shock loading, respectively. The shock wave velocity (D) and the particle velocity (u) could be derived as follows:

$$u = \sqrt{P(V_0 - V)}, \tag{33}$$

$$D = V_0\sqrt{P/(V_0 - V)}. \tag{34}$$

The shock Hugoniot D–u curves of dense and porous Al calculated from the new EOS are shown in Fig. 2, along with the experimental data[36–50] for comparison. The excellent agreement between the new EOS calculations and experimental data not only validates the models and parameterizations of the EOS thermal ion and electron components, but also demonstrates good applicability of the new EOS across wide thermodynamic and porosity regimes. Further, the shock Hugoniot P–ρ curves of dense and porous Al are calculated and presented in Fig. 3. For dense Al, the new EOS shows quantitative consistency with experimental results up to 10^6 GPa and 5-fold compression ratio. Meanwhile, for porous Al, it is for the first time the shock behaviors at wide pressure and temperature ranges are derived and presented. Notably, the initial porosity significantly affects the shock compression limits, which decrease rapidly as the porosity increases, indicating the profoundly excess heating effects of porous materials.

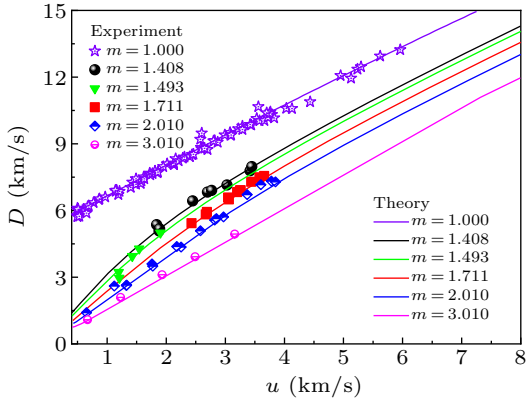


Fig. 2. Hugoniot D–u curves of dense and porous Al, where the lines are results derived from the new EOS, and dots are published experimental results.[36–50]

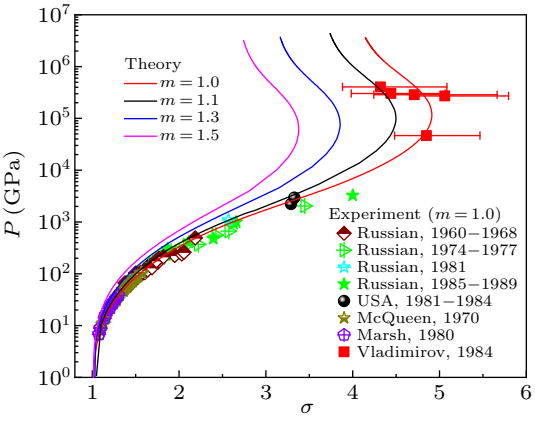


Fig. 3. Hugoniot P–σ curves of dense and porous Al, where the lines are result derived from the new EOS, and dots are published experimental results.[36–50]

3.3. Melting curves

The melting curve is an important reference data for validating the accuracy of the equation of state. As it is the intersection of the solid and liquid phase surfaces, both the models and parameters of the equation of state must be very accurate to reproduce the melting curve. In experiments, the melting curve is usually derived by temperature measurement and empirical models, while in theoretical equation of state, it is derived by solving the Gibbs free energy of solid and liquid phases under the same pressure and temperature.

In this part, the melting curve as well as the shock T–P curves of dense and porous Al are derived from the new EOS, as shown in Fig. 4. The melting curve of dense Al exhibits excellent agreement with experimental data,[51–53] demonstrating high accuracy of the new EOS. The overlapping of the melting and Hugoniot T–P curves indicates shock melting behaviors. As seen in Fig. 4, the shock-induced melting for dense Al takes place within a pressure range of 120–133 GPa, which agrees with the experimental results. As for porous Al, the shock-induced melting occurs at much lower temperature and pressure ranges, yet it still aligns with the melting curve of dense Al. These results are consistent with previous findings revealed by molecular dynamics simulations, which demonstrated that the porosity does not change the inherent thermodynamics of materials but shifts the thermodynamically response pathways under dynamical loading. The reproducing of the shock melting behavior of porous Al confirms the physical correctness of the new EOS.

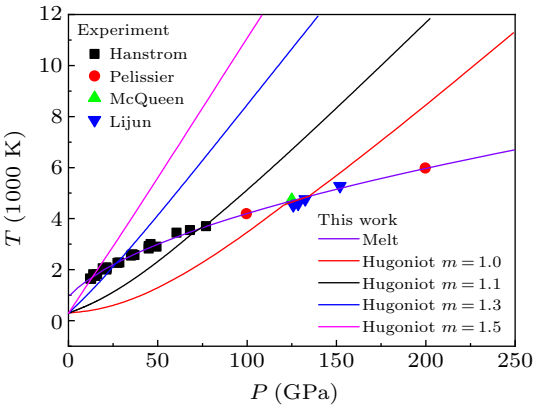


Fig. 4. Melting and Hugoniot T–P curves of dense and porous Al, where the lines are results derived from the new EOS, and dots are experimental results.[51–53]

4. Conclusion and perspectives

In this work, we presented a thermodynamically complete multi-phase equation of state, which is applicable to both dense and porous metals at wide ranges of temperature and pressure.

A standard three-term decomposition of the Helmholtz free energy as a function of specific volume and temperature is employed. For the cold component $F_c(V)$, models describing compression and expansion states are respectively constructed. For the thermal ion component $F_n(T,V)$, the Debye approximation is used for the models of solid phase, while the melting entropy is considered for the models of liquid phase. For the thermal electron component $F_e(T,V)$, the database calculated based on the TFK model is employed. These models enable the EOS applicable and robust at wide ranges of temperature and pressure. Meanwhile, the porosity of materials is modeled by introducing the dynamic porosity coefficient α and the constitutive P–α relation, connecting the thermodynamic properties between dense and porous systems. This allows for an accurate description of the volume decrease caused by void collapse, while maintaining the thermodynamic properties of porous systems identical to the dense ones.

A systematic evaluation of the new EOS is conducted with Al as an example. 300 K isotherm, shock Hugoniots, as well as melting curves of both dense and porous Al have been derived from the new EOS. The comparison of calculations with experimental data demonstrates good agreement, validating the effectiveness of the models and the accuracy of parameterizations. Given the applicability of new EOS at wide ranges of pressure, temperature and porosity, Hugoniot P–σ curves up to 10^6 GPa and shock melting behaviors of porous Al are for the first time derived by analytical EOS models, which predict much lower compression limit and shock melting temperatures than those of dense Al, respectively.

Acknowledgment

Project supported by the National Natural Science Foundation of China (Grant Nos. 12205023, U2230401, 12374056, U23A20537, and 11904027).

References

[1] Bushman A V 1992 *Intense dynamic loading of condensed matter* (CRC Press)
[2] Grüneisen E 1912 *Ann. Phys.* **344** 257
[3] Holzapfel W B, Hartwig M and Sievers W 2001 *J. Phys. Chem. Ref. Data* **30** 515
[4] More R M, Warren K H, Young D A and Zimmerman G B 1988 *Phys. Fluids* **31** 3059
[5] Birch F 1968 *Phys. Earth Planet. Inter.* **1** 141
[6] Lyon S P 1978 *Sesame: the Los Alamos National Laboratory equation of state database* LANL Rep
[7] Liu H, Song H, Zhang Q, Zhang G and Zhao Y 2016 *Matter Radiat. Extrem.* **1** 123
[8] Elkin V M, Mikhaylov V N, Ovechkin A A and Smirnov N A 2020 *J. Phys.: Condens. Matter* **32** 435403
[9] Cochrane K R, Kalita P, Brown J L, McCoy C A, Gluth J W, Hanshaw H L, Scoglietti E, Knudson M D, Rudin S P and Crockett S D 2022 *Phys. Rev. B* **105** 224109
[10] Medvedev A B 2014 *Shock Waves* **50** 582
[11] Lomonosov I V 2007 *Laser Part. Beams* **25** 567
[12] Benedict L X, Ogitsu T, Trave A, Wu C J, Sterne P A and Schwegler E 2009 *Phys. Rev. B* **79** 064106
[13] Benedict L X, Driver K P, Hamel S, Militzer B, Qi T, Correa A A, Saul A and Schwegler E 2014 *Phys. Rev. B* **89** 224109
[14] Dewaele A, Stutzmann V, Bouchet J, Bottin F, Occelli F and Mezouar M 2015 *Phys. Rev. B* **91** 134108
[15] Kalita P, Cochrane K R, Knudson M D, Ao T, Blada C, Jackson J, Gluth J, Hanshaw H, Scoglietti E and Crockett S D 2023 *Phys. Rev. B* **107** 94101
[16] Flanagan R M, Fensin S J and Meyers M A 2022 *Appl. Phys. Rev.* **9** 011305
[17] Wu Q and Jing F 1996 *J. Appl. Phys.* **80** 4343
[18] Song H F, Tian M F, Liu H F, Song H Z and Zhang G M 2014 *Chin. Phys. Lett.* **31** 016402
[19] Nayak B and Menon S V G 2018 *Phys. B* **529** 66
[20] Luo S, Jin B, Lutkenhaus J L and Nasrabadi H 2019 *Fluid Phase Equilib.* **498** 72
[21] Geng H, Tian H and Wu Q 2002 *J. Phys. Condens. Matter* **14** 10855
[22] Geng H, Wu Q, Tan H, Cai L and Jing F 2002 *J. Appl. Phys.* **92** 5924
[23] Nagayama K 2018 *J. Appl. Phys.* **57** 010301
[24] Nagayama K 2016 *J. Appl. Phys.* **119** 195901
[25] Cao X, Chen J, Yu Y and Wu Q 2018 *J. Appl. Phys.* **124** 215903

[26] Schlothauer T, Schimpf C, Schwarz M R, Heide G and Kroke E 2016 *J. Phys. Conf. Ser.* **774** 012053
[27] Yakushev V V, Utkin A V and Zhukov A N 2007 *AIP Conf. Proc.* **955** 205
[28] Kalita P, Cochrane K R, Knudson M D, Ao T, Blada C, Jackson J, Gluth J, Hanshaw H, Scoglietti E and Crockett S D 2023 *Phys. Rev. B* **107** 94101
[29] Bushman A V, Fortov V E, Lomonosov I V, Eliezer S and Ricci R A 1991 *Proc. Int. Sch. Phys.* p. 249
[30] Johnson J D 1991 *Int. J. High Press. Res.* **6** 277
[31] Xu X and Zhang W 1986 *Introduction to practical equation of states* (Science Press) (in Chinese)
[32] Herrmann W 1969 *J. Appl. Phys.* **40** 2490
[33] Carroll M and Holt A C 1972 *J. Appl. Phys.* **43** 759
[34] Nellis W J, Moriarty J A, Mitchell A C, Ross M, Dandrea R G, Ashcroft N W, Holmes N C and Gathers G R 1988 *Phys. Rev. Lett.* **60** 1414
[35] Dewaele A, Loubeyre P and Mezouar M 2004 *Phys. Rev. B* **70** 094112
[36] Glushak B L, Zharkov A P, Zhernokletov M V, Ternovoi V Y, Filimonov A S and Fortov V E 1989 *Zh. Eksp. Teor. Fiz* **96** 1301
[37] Trunin R F 1986 *Akad. Nauk SSSR. Fiz. Zemli* **2** 26
[38] Al'Tshuler L V, Bakanova A A, Dudoladov I P, Dynin E A, Trunin R F and Chekin B S 1981 *J. Appl. Mech. Tech. Phys.* **22** 145
[39] Van Thiel M, Shaner J, Salinas E and CALLNLAB 1977 Tech. report, LAWRENCE LIVERMORE Natl. LAB CA
[40] Al'tshuler L V and Chekin B S 1974 *Proceed. of 1st All-Union Pulsed Pressures Simposium* **1** 5
[41] Bakanova A A, Dudoladov I P and Sutulov Y N 1974 *J. Appl. Mech. Tech. Phys.* **15** 241
[42] McQueen R G, Marsh S P, Taylor J W, Fritz J N and Carter W J 1970 *High Veloc. impact Phenom.* **293** 294
[43] Isbell W M, Jones A H and Shipman F H 1968 *Hugoniot equation of state measurements for eleven materials to five megabars* (US Department of Commerce, National Technical Information Service)
[44] Skidmore I C and Morris E 1962 *Thermodyn. Nucl. Mater.* **6** 173
[45] Al'Tshuler L V, Kormer S B, Bakanova A A and Trunin R F 1960 *Sov. Phys. JETP* **11** 573
[46] Sirnonenko V A, Voloshin N P, Vladirnirov A S, Nagibin A P, Nogin V N, Popov V A, Vasilenko V A and Shoidin Y A 1985 *Sov. J. Exp. Theor. Phys.* **61** 869
[47] Ragan III C E 1984 *Phys. Rev. A* **29** 1391
[48] Ragan III C E 1982 *Phys. Rev. A* **25** 3360
[49] Mitchell A C and Nellis W J 1981 *J. Appl. Phys.* **52** 3363
[50] Marsh S P 1980 *LASL shock Hugoniot data vol. 5* (Univ of California Press)
[51] Hänström A and Lazor P 2000 *J. Alloys Compd.* **305** 209
[52] Pélissier J L 1984 *Phys. A* **128** 363
[53] McQueen R G, Fritz J N and Morris C E 1984 *Shock Waves in Condensed Matter 1983* (Am. Phys. Soc Press) p. 95
[54] Correa A A, Benedict L X, Young D A, Schwegler E and Bonev S A 2008 *Phys. Rev. B* **78** 024101
[55] Benedict L X, Ogitsu T, Trave A, Wu C J, Sterne P A and Schwegler E 2009 *Phys. Rev. B* **79** 064106
[56] Benedict L X, Driver K P, Hamel S, Militzer B, Qi T and Correa A A 2011 *Phys. Rev. B* **89** 224109